Handheld motion stabilized laser speckle imaging

BEN LERTSAKDADET,[1,2] **CODY DUNN,**[1,2,3] **ADRIAN BAHANI,**[1,2] **CHRISTIAN CROUZET,**[1,2] **AND BERNARD CHOI**[1,2,3,4,*]

[1]*Beckman Laser Institute and Medical Clinic, University of California-Irvine, 1002 Health Sciences Road East, Irvine, CA 92612, USA*

[2]*Department of Biomedical Engineering, University of California, Irvine, 3120 Natural Sciences II, Irvine, CA 92697, USA*

[3]*Edwards Lifesciences Center for Advanced Cardiovascular Technology, University of California, Irvine, 2400 Engineering Hall, Irvine, CA 92697, USA*

[4]*Department of Surgery, University of California, Irvine, 333 City Boulevard West, Suite 1600, Orange, CA 92868, USA*

[*]choib@uci.edu

Abstract: Laser speckle imaging (LSI) is a wide-field, noninvasive optical technique that allows researchers and clinicians to quantify blood flow in a variety of applications. However, traditional LSI devices are cart or tripod based mounted systems that are bulky and potentially difficult to maneuver in a clinical setting. We previously showed that the use of a handheld LSI device with the use of a fiducial marker (FM) to account for motion artifact is a viable alternative to mounted systems. Here we incorporated a handheld gimbal stabilizer (HGS) to produce a motion stabilized LSI (msLSI) device to further improve the quality of data acquired in handheld configurations. We evaluated the msLSI device *in vitro* using flow phantom experiments and *in vivo* using a dorsal window chamber model. For *in vitro* experiments, we quantified the speckle contrast of the FM (K_{FM}) using the mounted data set and tested 80% and 85% of K_{FM} as thresholds for useable images ($K_{FM,Mounted,80\%}$ and $K_{FM,Mounted,85\%}$). Handheld data sets using the msLSI device (stabilized handheld) and handheld data sets without the HGS (handheld) were collected. Using $K_{FM,Mounted,80\%}$ and $K_{FM,Mounted,85\%}$ as the threshold, the number of images above the threshold for stabilized handheld (38 ± 7 and 10 ± 2) was significantly greater ($p = 0.031$) than for handheld operation (16 ± 2 and 4 ± 1). We quantified a region of interest within the flow region (K_{FLOW}), which led to a percent difference of $8.5\% \pm 2.9\%$ and $7.8\% \pm 3.1\%$ between stabilized handheld and handheld configurations at each threshold. For *in vivo* experiments, we quantified the speckle contrast of the window chamber (K_{WC}) using the mounted data set and tested 80% of K_{WC} ($K_{WC,Mounted,80\%}$). Stabilized handheld operation provided 53 ± 24 images above $K_{WC,Mounted,80\%}$, while handheld operation provided only 23 ± 13 images. We quantified the speckle flow index (SFI) of the vessels and the background to calculate a signal-to-background ratio (SBR) of the window chamber. Stabilized handheld operation provided a greater SBR (2.32 ± 0.29) compared to handheld operation (1.83 ± 0.21). Both the number of images above threshold and SBR were statistically significantly greater in the stabilized handheld data sets ($p = 0.0312$). These results display the improved usability of handheld data acquired with an msLSI device.

1. Introduction

Laser speckle imaging (LSI) is a wide-field, noninvasive optical technique that allows researchers and clinicians to quantify blood flow in a variety of applications. In a research setting, some applications of LSI include measuring blood flow in the rodent brain during externally stimulated conditions [1], measuring blood flow in a window chamber as a response to therapies [2–4], and

measuring blood flow in varying severities of induced burn wounds [5,6]. In a clinical setting, LSI can also provide assistance in assessing medical conditions such as peripheral vascular disease [7], diabetes [8], and burn wounds at the bedside through measured blood flow [9].

The widespread use of LSI in the clinic has been hindered by the bulky form factor of currently available LSI devices such as cart or tripod mounted systems. These devices can be cumbersome and difficult to maneuver in a crowded hospital setting, thus motivating design of new LSI devices with increased portability and convenience. A potential solution for portable clinical blood flow imaging is a handheld LSI device [10]. We previously demonstrated that a handheld LSI device enables the collection of meaningful data if issues related to motion artifact are properly addressed [11].

Two concerns of handheld LSI are image misalignment and motion artifact (Fig. 1). Figure 1(a) and (b) shows the average speckle contrast image obtained using multiple images (n = 150) from a mounted configuration during an *in vitro* flow phantom experiment (Section 2.3) and an *in vivo* window chamber measurement (Section 2.4). However, in handheld data sets, image misalignment and motion artifact make the average speckle contrast image unusable (Fig. 1c-f). Both of these can be addressed by using a fiducial marker (FM) [11], with which we can account for motion artifact by sorting through images to identify frames with the least amount of motion artifact. To account for issues with image misalignment, we can use the fiducial marker to co-register images to more effectively produce average blood flow maps, or speckle flow index (SFI) images.
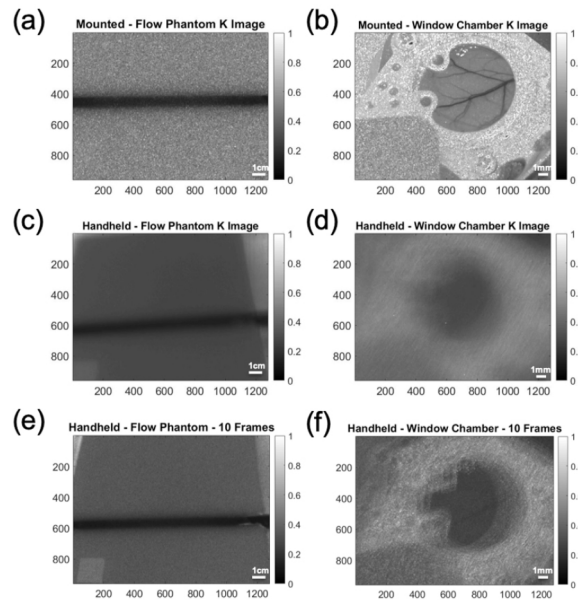

Fig. 1. Motion artifact during data acquired using laser speckle imaging (LSI) device in mounted and handheld configurations. An average speckle contrast (K) image (n = 150) from a mounted configuration data set of (a) an *in vitro* flow phantom measurement and (b) an *in vivo* window chamber measurement are shown. In comparison, a sample data set acquired in a handheld configuration in (c) an *in vitro* flow phantom measurement and (d) an *in vivo* window chamber measurements shows reduced K values affected by motion artifact during data acquisition. In (d), the loss of visualization of the blood vessels within the window chamber is due to motion artifact (See **Visualization 1**). (e, f) Even when using an average of 10 frames to create an average K image, there is a noticeable reduction in sharpness in the (e) flow tube in the flow phantom and (f) a loss of vascular visibility in the window chamber.

In addition to the use of a FM, here we propose use of a handheld gimbal stabilizer (HGS) to further reduce motion artifact associated with data acquired in a handheld manner. An HGS is commonly used in video recording to reduce vibrations and shakiness when holding cameras. It utilizes motors to account for motion on multiple axes, and a 3-axis HGS can ensure the motion of the camera remains independent of the user. Paradoxically, a limitation of using an HGS occurs when there is a lack of movement. The vibration caused by the motors may add motion artifact in mounted data sets, so it is best used in a handheld manner. We hypothesize that by pairing a LSI system with a HGS, we can further reduce motion artifact than LSI in a handheld manner.

In this work we show that a handheld gimbal stabilized LSI device, which we refer to as our motion stabilized LSI (msLSI) device, reduces motion artifact when acquiring data in a handheld manner. This leads to an increased number of useable frames above our predefined threshold, which was determined from our mounted data sets. We validate the improved motion artifact correction in both *in vitro* flow phantom experiments and *in vivo* dorsal window chamber measurements.

2. Materials and methods

2.1. Motion stabilized laser speckle imaging (mSLSI) device

The LSI device consisted of an 8-bit, 1.32 megapixel CCD camera (CMLN-13S2M-CS, FLIR Integrated Imaging Solutions, Inc., Richmond, BC, Canada, pixel size = 3.75μm), a variable zoom C-mount lens (Computar C-Mount 13-130 mm Varifocal Lens, Computar, Cary, NC), and 809 nm near-infrared laser diode (140 mW, Ondax Inc., Monrovia, CA). The laser was attached to the camera and lens setup with a custom 3D-printed camera mount. The imaging system acquired 1280×960 pixel frames at 15 Hz, which resulted in a field of view (FOV) of approximately 140 mm x 105 mm (4:3 ratio). The imaging system was attached to a HGS (Crane v2 3-Axis Handheld Gimbal Stabilizer, Zhiyun-Tech) to create the msLSI device (Fig. 2). The msLSI device was connected to a tablet computer (Surface Pro 2, Microsoft Inc.) via a six-foot-long A-Male to Mini-B USB cable. Data were collected using the FlyCap2 Software (FLIR Integrated Imaging Solutions, Inc., Richmond, BC, Canada) and processed using custom code written in MATLAB (The Mathworks, Natick MA).

Fig. 2. Motion Stabilized Laser Speckle Imaging (msLSI) Device. Fully-assembled device utilizing a gimbal stabilizer with the LSI device.

2.2. Fiducial Marker (FM) Identification

To test motion artifact reduction, the imaging system was used in a handheld manner both with and without the HGS. The setup for each configuration was similar in weight to mitigate effects of weight alone on handheld operation. We ensured the Nyquist sampling criterion [12] was satisfied at all magnifications with the LSI device. A spatial processing algorithm was used to convert all raw images to speckle contrast images. The spatial processing algorithm utilized a 7×7 pixel sliding window with the relationship $K = \sigma/<I>$ calculated for each sliding window position. K is the local speckle contrast, σ the standard deviation of the pixel intensities within the window, and $<I>$ the mean intensity of the pixels within the window. As previously described in [11], a FM made from an 18% grey card, (Neewer, model #10079934) commonly used to correct for white balance in photography, was incorporated into the imaging protocol. We utilized this FM for thresholding and image co-registration [11]. Custom written MATLAB code identified the FM in each frame and quantified the speckle contrast of the fiducial marker (K_{FM}) (Fig. 3). Images within each data set were then sorted based on K_{FM}. Using the mounted LSI data, we considered thresholds of 80, 85, and 90% of the K_{FM} measured with a mounted configuration ($K_{FM,Mounted,80\%}$ and $K_{FM,Mounted,85\%}$, respectively) to identify the images deemed acceptable from each handheld data set. However, since the 90% K_{FM} threshold did not yield any useable frames in a majority of the data sets, we proceeded with only 80% and 85% thresholds for K_{FM}. Custom MATLAB code automatically co-registered these images in each data set to create an average K image (Fig. 3). Regions of interest (ROIs) within the flow region were selected using the average speckle contrast image (K_{FLOW}).
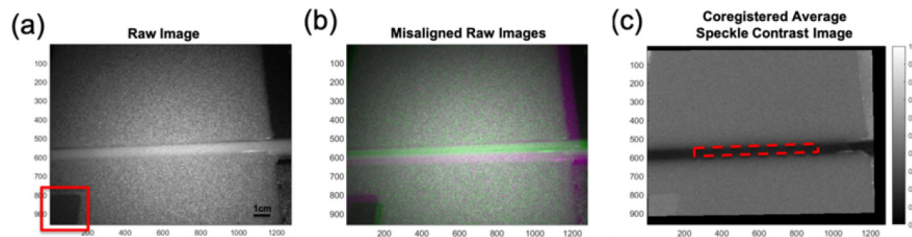

Fig. 3. Workflow to co-register each speckle contrast (K) image contained within a sequence of images. (a) Representative raw speckle image. The fiducial marker (denoted by red box) in each raw image is identified and the mean K value of the marker (K_{FM}) calculated. (b) False-color image showing degree of misalignment among raw images. Green and purple shading of pixels is used to highlight the co-registered and misaligned images, respectively. (c) After identifying the K images with K_{FM} values above a threshold K_{FM} value (see text for more details), the misaligned images are aligned and cropped to produce a final co-registered average K image. An ROI within the dynamic flow region was selected (in red) for further quantitative analysis.

2.3. In vitro flow phantom experiment

To test the hypothesis that msLSI performs better than handheld LSI, we performed an *in vitro* flow phantom experiment using the LSI device in four configurations: 1) mounted, 2) mounted with gimbal stabilizer (stabilized mounted), 3) handheld, and 4) handheld with gimbal stabilizer (stabilized handheld). The FOV of the device was set to ~140 mm x 105 mm (4:3 ratio) and the exposure time of the camera set to 10 ms. We used a solid silicone phantom with a surface-level inclusion flow tube (inner diameter 10 mm). The flow medium was a 1% Intralipid solution (Fresenius Kabi, Lake Zurich, IL) that was infused into the tube using a mechanical pump (NE-1000 Single Syringe Pump, Pump Systems Inc.). The flow speed of the solution was changed

from 0 mm/s to 5 mm/s in 1 mm/s increments. Sequences of 150 images were acquired with all configurations.

To compare the differences in stability due to the hardware change of acquiring data with or without the HGS, we acquired data using each of the four configurations. We then determined the number of images with K_{FM} greater than $K_{FM,Mounted,80\%}$ and $K_{FM,Mounted,85\%}$ in the handheld and stabilized handheld data sets. Although the number of images above each threshold was different, we used the number of images determined in the stabilized handheld data sets to create the average speckle contrast images for both the handheld and stabilized handheld configurations. This was done to remove biases associated with using differing number of images to create the average speckle contrast image. For handheld and stabilized handheld configurations, multiple users (n = 4) operated the device. The resulting values from each of the users were averaged to represent each flow condition (6 flow conditions, 0-5mm/s in 1mm/s increments).

2.4. In vivo dorsal window chamber experiment

As a demonstration, we collected LSI data of the microcirculation from a mouse dorsal window chamber. The animal surgery was carried out according to the protocol outlined in [2] and was performed under protocol AUP-17-074 approved by the Institutional Animal Care and Use Committee at University of California, Irvine. The animal was anesthetized using isoflurane (2%, balance oxygen) and the LSI device used to acquire data with each of the four previously mentioned configurations. The window chamber consisted of a 10 mm viewing window of the microvascular network on the subdermal side of an intact skin layer.

To account for the smaller features of the window chamber model, the FOV of the LSI device was changed to approximately 20 mm x 15 mm. An exposure time of 5 ms was used to account for the expected difficulties in imaging a considerably smaller FOV. Sequences of 150 images were acquired with each configuration.

Since each frame in a data sequence may have varying amounts of motion artifact, custom MATLAB code was written to account for these fluctuations in K and automate identification of the window chamber in each image (Fig. 4). We first utilized a scanning quantile to account for the dynamic K images. Using quantiles allows us to scan each image column-wise and row-wise and sort the K of each pixel [13]. In doing so, we can identify the location of the tissue within the window chamber since the K associated with the tissue differs from the K associated with the titanium window chamber (Fig. 4(a), (b)). By multiplying the row-wise and column-wise quantile images, we increased the contrast between the tissue and the window chamber (Fig. 4(c)). Since we expected the tissue region within the window chamber to have a lower K, we were able to identify the window chamber after thresholding the quantiled image (Fig. 4(d)). The resultant threshold image was inverted to create a mask of the tissue region within the window chamber (Fig. 4(e)). A size threshold was applied to remove smaller masked regions that were not the tissue region (Fig. 4(f)). A fill was performed to create a solid mask for blob counting-based identification of a circular region (Fig. 4 (g)). The tissue region was identified and a logical mask created (Fig. 4 (h), (i)). Using the logical mask, we created a masked K image showing only the tissue region within the window chamber, which we used for co-registration (Fig. 4j).

For the *in vivo* experiments, multiple users (n = 6) acquired data with the LSI device in stabilized handheld and handheld configurations. We used the tissue region within the window chamber frame as the FM. The mean speckle contrast value of the tissue was calculated as the threshold (K_{WC}). We first determined $K_{WC,Mounted}$ using the mounted data set. We then calculated the 80% threshold of K_{WC} ($K_{WC,Mounted,80\%}$) and applied this threshold to the handheld and stabilized handheld data sets to determine the number of frames whose K_{WC} was above the threshold. These images were used for co-registration and calculation of an average speckle contrast image for the window chamber. This image was then converted into speckle flow index (SFI) images using a simplified speckle imaging equation $SFI = 1/(2*K^2*T)$. [14]. SFI has been
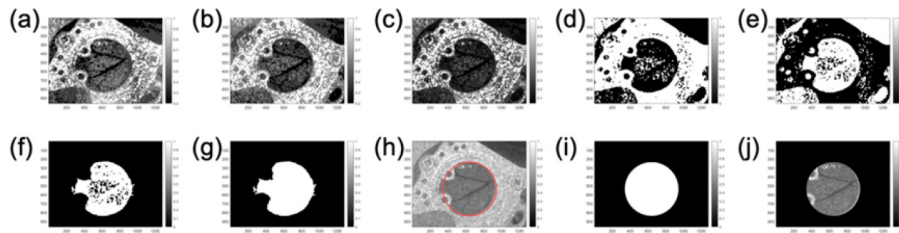
Fig. 4. Automated identification of mouse dorsal window chamber from raw speckle image sequence. (a) Column-wise quantile speckle contrast (K) image (b) Row-wise quantile K image (c) Multiplied column-wise and row-wise K image (d) Binarization of multiplied K image (e) Inverted binarized image (f) Feature removal of smaller regions (g) Filled remaining feature (h) Circular geometric identification of tissue within window chamber (i) Masked image using identified circle (j) Masked K image showing the window chamber (see **Visualization 2**).

shown to correlate linearly with blood flow over the flow speeds observed in the window chamber [13,14]. Lastly, we select an ROI within the vessel and an ROI of the background tissue to quantify the mean SFI value of the signal (vessel) and background, respectively. These mean SFI values are used to quantify the signal-to-background ratio (SBR).

2.5. Statistical analysis

All handheld and stabilized handheld data were treated as paired data since the same users were involved in each group. As such, a Wilcoxon matched-pairs signed rank test was used to test the statistical significance of both the number of images with K_{FM} or K_{WC} above the set threshold and the SBR between handheld and stabilized handheld data sets. We considered p-value < 0.05 to be significant, and significance is denoted by * on the relevant figures.

3. Results

3.1. In vitro flow phantom experiment

Both the mounted and stabilized mounted data sets resulted in all images with K_{FM} above the $K_{FM,Mounted,80\%}$ and $K_{FM,Mounted,85\%}$ thresholds. The number of images above $K_{FM,Mounted,80\%}$ and $K_{FM,Mounted,85\%}$ was significantly greater in the stabilized handheld data set than in the handheld data sets (p = 0.031). Using $K_{FM,Mounted,80\%}$, the number of images above the threshold with handheld and stabilized handheld operation were 16 ± 2 and 38 ± 7, respectively (Fig. 5(a)). Using $K_{FM,Mounted,85\%}$, the number of images above the threshold with handheld and stabilized handheld were 4 ± 1 and 10 ± 2, respectively (Fig. 5(b)). K_{FLOW} was greater with stabilized handheld operation than with handheld operation in all data sets (Fig. 5(c)). The mean percent difference in K_{FLOW} between the handheld and stabilized handheld data sets across all flow speeds using $K_{FM,Mounted,80\%}$ and $K_{FM,Mounted,85\%}$ were 8.5% ± 2.9% and 7.8% ± 3.1%, respectively.

3.2. In vivo window chamber experiment

After identifying the window chamber using the workflow outlined in Fig. 4, we applied the $K_{WC,Mounted,80\%}$ threshold and quantified the number of images in each data set above this threshold. The number of images above $K_{WC,Mounted,80\%}$ was greater in the stabilized handheld data sets compared to the handheld data sets (Fig. 6). Using the msLSI device provided handheld data sets and stabilized handheld data sets provided 23 ± 13 and 54 ± 24 images, respectively(Fig. 6(a)). The greater number of images above the threshold in the stabilized handheld data set was statistically significant (p = 0.0312). We co-registered the images based on
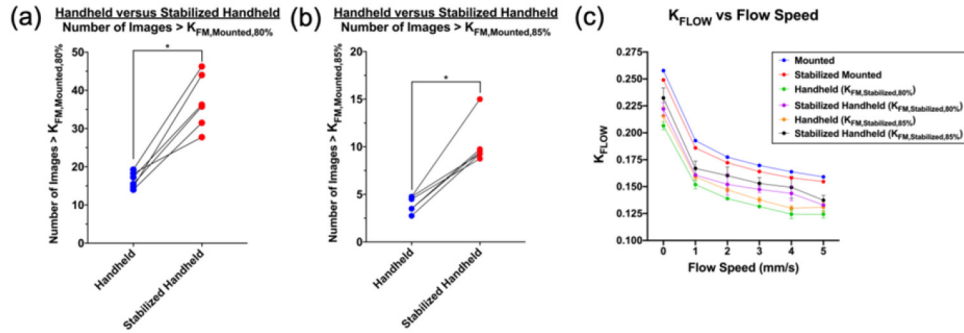
Fig. 5. A handheld gimbal stabilizer (HGS) significantly improves the performance of handheld LSI. The mounted speckle contrast of the fiducial marker (K_{FM}) was quantified and used to set either an 80% and 85% threshold ($K_{FM,Mounted,80\%}$ and $K_{FM,Mounted,85\%}$, respectively). We then determined the number of images in handheld and stabilized handheld data sets with K_{FM} above these thresholds. (a, b) The number of images above $K_{FM,Mounted,80\%}$ and $K_{FM,Mounted,85\%}$ in the stabilized handheld data sets was significantly greater than for the handheld data sets ($p = 0.031$). With mounted and stabilized mounted configurations, the value of K_{FM} for each image in the entire image sequence (150 images) was above 80% K_{FM}. (c) The speckle contrast within the flow region (K_{FLOW}) of the tissue phantom was greater with stabilized handheld than with handheld operation across all flow speeds when using both $K_{FM,Mounted,80\%}$ and $K_{FM,Mounted,85\%}$, which resulted in a 8.5% ± 2.9% and 7.8% ± 3.1% percent differences, respectively. Error bars are not shown when the errors for each data point are smaller than the symbol used to represent that data.
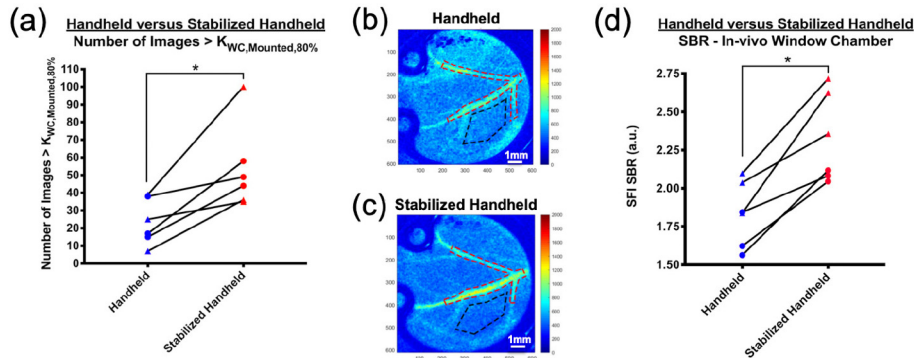

Fig. 6. Use of a gimbal stabilizer improves the performance of handheld laser speckle imaging for imaging microvasculature within a small region of interest (ROI). (a) The number of handheld images with a window-chamber speckle contrast above 80% was determined. The mean and standard deviation of number of images above threshold in the handheld and stabilized handheld data sets were 23 ± 13 and 54 ± 24, respectively. The greater number of images above the threshold in the stabilized handheld data set was statistically significant ($p = 0.0312$). Representative mean speckle flow index (SFI) images from a single user for handheld (b) and stabilized handheld data (c) sets show that handheld operation leads to a higher SFI (i.e., noise) in the background. ROIs of the vessel (red) and background (black) are outlined. (d) The mean and standard deviation of the signal-to-background ratio for handheld and stabilized handheld data sets were 1.83 ± 0.21 and 2.32 ± 0.29. The greater SBR in stabilized handheld was also statistically significant. The different symbols indicate the different window chambers imaged.

the window chamber and created an average SFI image for each data set (Fig. 6(b), (c)). The SBR of the SFI images were quantified using the SFI value within a ROI of the vessels over the SFI value of a static background ROI. A higher SBR is associated with reduced motion artifact. The SBR in the handheld data sets was 1.83 ± 0.21 compared to 2.32 ± 0.29 in stabilized handheld data sets (Fig. 6(d)). The SBR was statistically significantly greater in stabilized handheld.

4.   Discussion

LSI can be applied to a wide range of pre-clinical and clinical studies [1–4,10,13–18]. However, a portable device is desirable for clinical applications where space is limited. For example, a handheld LSI device is a potential solution for clinical blood flow imaging at the bedside. In our previous study, we showed the viability of using LSI in a handheld manner [10,11]. Other handheld LSI devices have been created, but the primary application space is for retinal blood flow imaging [19]. In this study, data acquisition is described as occurring with a "stabilized" configuration; however, the stabilized method the authors refer to involves attaching their handheld LSI device to a rigid mount on a table. Our stabilized approach is novel in that we are using a HGS in both a handheld configuration and a mounted configuration. By incorporating a HGS into the LSI device, we demonstrated that msLSI can further reduce motion artifact when performing handheld LSI.

Stabilized handheld data sets provided significantly more frames above $K_{FM,Mounted,80\%}$ and $K_{FM,Mounted,85\%}$ thresholds compared to handheld operation alone. Since all data sets contained the same number of images, stabilized handheld data resulted in a higher rate of useable frames. This can reduce imaging times by allowing a lower number of frames acquired using stabilized handheld operation but resulting in the same number of useable frames as handheld operation. By reducing data acquisition times and motion artifact, stabilized handheld LSI becomes a more viable option for clinical use compared to bulky conventional LSI devices.

An additional consideration for clinical blood flow imaging is the desired FOV for specific applications. Hence, LSI devices used in clinical studies have a large range of FOV. The Pericam PSI device provided a 120 mm x 120 mm FOV when imaging scald burn in patients, while a LSI dermascope provided a 5 mm x 3.75 mm while measuring skin lesions [9,14]. Using a smaller FOV amplifies motion artifact, making it less feasible for non-contact handheld LSI. However, when we reduced the FOV of the msLSI device from 140 mm x 105 mm to 20 mm x 15 mm, we still demonstrated an improved SNR in the stabilized handheld configuration that was statistically significantly greater than unstabilized handheld.

For *in vivo* experiments with the dorsal window chamber model, the region we selected as background is not a true static background; indeed, it contains microvasculature that were not individually resolved by our optical system. Flow changes within these small vessels may affect the SFI of the selected background ROI. To investigate this further, we analyzed a sequence of 150 SFI images collected from the window chamber shown in Fig. 6, using the LSI system in a mounted configuration. We focused on this configuration because it provides a best-case estimate of SBR stability of the *in vivo* model. We quantified the mean and standard deviation of the SFI values in ROIs selected from within a vessel and a background region, and calculated a coefficient of variation (CV, quotient of standard deviation and mean) of 1) SFI in each of the two regions and 2) SBR for each of the 150 images. The CV for the vessel and background regions was 10 and 18%, respectively. The CV of the SBR values was 10%. Since the mean SBR in the stabilized handheld configuration was 27% higher than the mean SBR in the unstabilized handheld configuration, we believe that the improvement offered by stabilized handheld operation is significant, even given the uncertainty associated with fluctuations in background SFI value associated with capillary-level perfusion of the region.

Although we have shown that msLSI is a viable alternative to conventional LSI systems for clinical use, there are some limitations to consider. A fiducial marker is needed because motion

artifact can occur due to user or subject movement, and the fiducial marker is required to quantify movement and align frames. Without a fiducial marker, with our current approach we would be unable to identify useable frames or realign images. By incorporating a HGS to a handheld LSI device, we increase both overall cost and weight of the system. The added weight may make it more difficult to steadily operate. However, we plan to address this in future generations of the device by miniaturizing the LSI device and HGS. Another limitation of handheld LSI is the inherent motion due to using the device in a handheld manner, which will decrease K in an entire image. We plan to account for this by continuing to utilize a FM in the imaging protocol.

In summary, we further displayed the potential for handheld LSI by introducing evaluation of a msLSI device. We validated the improved stability and reduced motion artifact in both *in vitro* and *in vivo* experiments with multiple users. We varied the FOV of the device and showed that msLSI can provide useable blood flow maps even at smaller FOV where motion artifact is amplified. The msLSI approach is a viable alternative to conventional LSI devices for a variety of clinical applications. Future studies will involve evaluation of the msLSI device for clinical blood flow measurements.

Funding

Acknowledgements

Disclosures

The authors declare that there are no conflicts of interest related to this article.

References

1. C. Crouzet, R. H. Wilson, A. Bazrafkan, M. H. Farahabadi, D. Lee, J. Alcocer, B. J. Tromberg, B. Choi, and Y. Akbari, "Cerebral blood flow is decoupled from blood pressure and linked to EEG bursting after resuscitation from cardiac arrest," Biomed. Opt. Express **7**(11), 4660 (2016).
2. A. J. Moy, S. M. White, E. S. Indrawan, J. Lotfi, M. J. Nudelman, S. J. Costantini, N. Agarwal, W. Jia, K. M. Kelly, B. S. Sorg, and B. Choi, "Wide-field functional imaging of blood flow and hemoglobin oxygen saturation in the rodent dorsal window chamber," Microvasc. Res. **82**(3), 199–209 (2011).
3. W. J. Moy, S. J. Patel, B. S. Lertsakdadet, R. P. Arora, K. M. Nielsen, K. M. Kelly, and B. Choi, "Preclinical In Vivo Evaluation of Npe6-Mediated Photodynamic Therapy on Normal Vasculature," Lasers Surg. Med. **44**(2), 158–162 (2012).
4. K. M. Kelly, W. J. Moy, A. J. Moy, B. S. Lertsakdadet, J. J. Moy, E. Nguyen, A. Nguyen, K. E. Osann, and B. Choi, "Talaporfin Sodium-Mediated Photodynamic Therapy Alone and in Combination with Pulsed Dye Laser on Cutaneous Vasculature," J. Invest. Dermatol. **135**(1), 302–304 (2015).

5. A. Ponticorvo, D. M. Burmeister, B. Yang, B. Choi, R. J. Christy, and A. J. Durkin, "Quantitative assessment of graded burn wounds isn a porcine model using spatial frequency domain imaging (SFDI) and laser speckle imaging (LSI)," Biomed. Opt. Express **5**(10), 3467–3481 (2014).

6. A. Ponticorvo, D. M. Burmeister, R. Rowland, M. Baldado, G. T. Kennedy, R. Saager, N. Bernal, B. Choi, and A. J. Durkin, "Quantitative long-term measurements of burns in a rat model using Spatial Frequency Domain Imaging (SFDI) and Laser Speckle Imaging (LSI)," Lasers Surg. Med. **49**(3), 293–304 (2017).

7. S. Katsui, Y. Inoue, K. Igari, T. Toyofuku, and T. Kudo, "Novel Assessment Tool Based on Laser Speckle Contrast Imaging to Diagnose Severe Ischemia in the Lower Limb for patients with peripheral arterial disease," Lasers Surg. Med. **49**(7), 645–651 (2017).

8. A. S. de M. Matheus, E. L. S. Clemente, M. de Lourdes Guimarães Rodrigues, D. C. Torres Valença, and M. B. Gomes, "Assessment of microvascular endothelial function in type 1 diabetes using laser speckle contrast imaging," J. Diabetes Complications **31**(4), 753–757 (2017).

9. R. Mirdell, F. Iredahl, F. Sjöberg, S. Farnebo, and E. Tesselaar, "Microvascular blood flow in scalds in children and its relation to duration of wound healing: A study using laser speckle contrast imaging," Burns **42**(3), 648–654 (2016).

10. R. Farraro, O. Fathi, and B. Choi, "Handheld, point-of-care laser speckle imaging," J. Biomed. Opt. **21**(9), 094001 (2016).

11. B. Lertsakdadet, B. Y. Yang, C. E. Dunn, A. Ponticorvo, C. Crouzet, N. Bernal, A. J. Durkin, and B. Choi, "Correcting for motion artifact in handheld laser speckle images," J. Biomed. Opt. **23**(03), 1 (2018).

12. S. J. Kirkpatrick, D. D. Duncan, and E. M. Wells-Gray, "Detrimental effects of speckle-pixel size matching in laser speckle contrast imaging," Opt. Lett. **33**(24), 2886–2888 (2008).

13. "Quantiles." [Online]. Available: https://www.statsdirect.com/help/nonparametric_methods/quantiles.htm. [Accessed: 23-Jan-2019].

14. B. Choi, J. C. Ramirez-san-juan, J. Lotfi, and J. S. Nelson, "Linear response range characterization and in vivo," J. Biomed. Opt. **11**(4), 041129 (2006).

15. S. M. White, M. Valdebran, K. M. Kelly, and B. Choi, "Simultaneous Blood Flow Measurement and Dermoscopy of Skin Lesions Using Dual-Mode Dermascope," Sci. Rep. **8**(1), 16941 (2018).

16. B. Yang, O. Yang, J. Guzman, P. Nguyen, C. Crouzet, K. E. Osann, K. M. Kelly, J. S. Nelson, and B. Choi, "Intraoperative, real-time monitoring of blood flow dynamics associated with laser surgery of port wine stain birthmarks," Lasers Surg. Med. **47**(6), 469–475 (2015).

17. O. Yang and B. Choi, "Laser speckle imaging using a consumer-grade color camera," Opt. Lett. **37**(19), 3957–3959 (2012).

18. C. E. Dunn, B. Lertsakdadet, C. Crouzet, A. Bahani, and B. Choi, "Comparison of speckleplethysmographic (SPG) and photoplethysmographic (PPG) imaging by Monte Carlo simulations and *in vivo* measurements," Biomed. Opt. Express **9**(9), 4306–4316 (2018).

19. A. Rege, S. I. Cunningham, Y. Liu, K. Raje, S. Kalarn, J. Brooke, L. Schocket, S. Scott, A. Shafi, L. Toledo, and J. Osamah, "Noninvasive Assessment of Retinal Blood Flow Using a Novel Handheld Laser Speckle Contrast Imager," Trans. Vis. Sci. Tech. **7**(6), 7 (2018).